

Progressive Learning Algorithm for Efficient Person Re-Identification

Zhen Li Hanyang Shao
 Shanghai Glotech Information Technology Pte. Ltd
 Nanjing University of Aeronautics and Astronautics

lizh0019@gmail.com

Hy.shao@grandhonor.net

Nian Xue Liang Niu
 New York University
 nian.xue@nyu.edu liang.niu@nyu.edu

LiangLiang Cao
 University of Massachusetts Amherst
 llcao@cs.umass.edu

Abstract

This paper studies the problem of Person Re-Identification (ReID) for large-scale applications. Recent research efforts have been devoted to building complicated part models, which introduce considerably high computational cost and memory consumption, inhibiting its practicability in large-scale applications. This paper aims to develop a novel learning strategy to find efficient feature embeddings while maintaining the balance of accuracy and model complexity. More specifically, we find by enhancing the classical triplet loss together with cross-entropy loss, our method can explore the hard examples and build a discriminant feature embedding yet compact enough for large-scale applications. Our method is carried out progressively using Bayesian optimization, and we call it the Progressive Learning Algorithm (PLA). Extensive experiments on three large-scale datasets show that our PLA is comparable or better than the-state-of-the-arts. Especially, on the challenging Market-1501 dataset, we achieve Rank-1=94.7%/mAP=89.4% while saving at least 30% parameters than strong part models.

1. Introduction

One key challenge in person re-identification (ReID) is how to balance the tradeoff between accuracy and model complexity. Person ReID aims to retrieve a given person across a vast amount of videos, despite significant variations under different surveillance cameras at different locations. Some research studies [31, 34] have obtained the-state-of-the-art accuracy on public datasets, at the cost of increasing computational complexity and a large number of parameters. For example, MGN [34] splits the network into one branch for global feature and two other branches for local features, resulting in 180MB inference memory per image

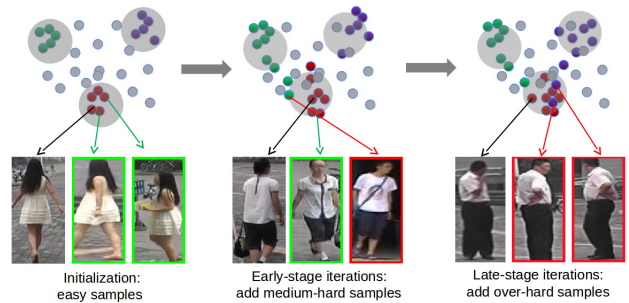


Figure 1. Training mini-batches consisting of easy, medium-hard and over-hard examples. A red box indicates a person that is different from the anchor sample, while a green box indicates the same person. The hard examples are valuable to train a high precision model but may lead to confusion in the optimization. We propose progressive learning strategy to solve this challenge, which first learn easy and medium-hard examples. Note that training on over-hard examples are circumvented if they are less beneficial than medium-hard ones.

(or 23GB per batch of 128 images) which prevents it from being used on resource-constrained platforms [8]. Another group of methods [30, 7, 14] focus on scalable solutions that can support real-time search across hundreds of hours of videos, with simpler network and compact representation. However, the performance of the second group degenerates quickly with the simpler model structure.

The goal of this paper is to learn an efficient model for person ReID that can match the-state-of-the-art performance. With the recent success [22], triplet loss is preferred by many researchers because it does not require the images of the sample person to collapse to a single cluster, so they can potentially model the variations and different parts of the same person. However, triplet loss mainly focuses on the question of “how similar are the two images” [7] instead of “is this a new person”, and often suffers from a weaker generalization capability. In this paper, we be-

lieve triplet loss and cross-entropy loss are complementary to each other, and propose to integrate two loss into one framework.

In practice, optimizing triplet loss at large scale is not easy due to the difficulty of sampling good candidates of hard triplets. When combining triplet loss with cross-entropy loss, the optimization using stochastic gradient descents becomes more difficult. A straightforward optimization may find an inferior solution or even fail to converge. If we choose all the easy examples, the model may not be discriminant enough. But if we choose all hard examples, it will make it difficult for the SGD optimizer to get out of the local minimum, and the model may stop improving in the early stage.

We believe the key to solve the difficult optimization problem is to train the model in a progressive way. At the beginning of the stochastic optimization process, we get more simple samples in every batch, to make sure that most of them could be recognized correctly. In the later, we focus on the hard examples, and reduce the number of simple samples. The resulted algorithm is to progressively learn the triplet loss from simple samples to hard samples using the Bayesian framework. We call this new approach as Progressive Learning Algorithm (PLA). Fig. 1 shows the progressive learning in different strategies. This approach can help to optimize not only triplet loss but also the new composite loss for ReID problems.

Using the framework of PLA, this paper found an efficient way to integrate different branches in the ReID network structure. We used one shared convolutional network (i.e., the ResNet-50 [6]) for each image. Note that almost all previous works used different convolutional networks for separate branches. The proposed architecture significantly reduces the computational cost and model complexity. The backbone is not altered and the feature maps after global pooling are fed to 1×1 convolution, producing two global features which are evaluated using cross-entropy loss and triplet loss, respectively. It is convenient to deploy the inference model due to its compact nature.

Our approach enjoys a good balance of model complexity and accuracy. Our model is almost as efficient as ResNet-50 based DaRe [36], and can finish inference (batch size 128) of 17,000 images in a second, using 1 GTX 1080Ti card, while still obtaining comparable accuracy with the-state-of-the-arts. On the challenge Market1501 dataset, our single query model without reranking achieves the Rank-1 score of 93.7%.

This paper is structured as follows. In Section 2, we review the related works. The proposed PLA is elaborated in Section 3, followed by the extensive experiments in Section 4 which validate the superiority of PLA in the balance of accuracy and resource requirement. Finally, Section 5 concludes this work.

2. Related Work

Deep learning models for ReID can be categorized into global models and part models. Global models utilize only global features, typically after global pooling operations, without analyzing regions of feature maps. In contrast, part models typically learn various local features in spatial domain of feature maps.

2.1. Global model

Based on a standard backbone of deep neural network such as ResNet-50 [6], the loss function can be designed to optimize the CNN weights. A classification loss is an early choice [3, 44, 46, 13]. Many works [3, 44, 13], consider a multi-task objective functions to update the CNN weights. These approaches train a deep CNN with the cross-entropy loss or integrate it with other losses, and then use the network as a feature extractor, followed by combining it with a metric learning approach to produce final ReID features. For instance, in [30], each weight vector within a fully connected layer with classification loss as a projection basis are decorrelated using Singular Vector Decomposition (SVD), and the Rank-1 accuracy is improved from 73.8% to 82.3% on the Market-1501 dataset. However, under such framework, the number of learnable weights increases in proportion to the number of identities, while most of them will be not be used in model inference.

A breakthrough for the ReID task is FaceNet [22] where a convolutional neural network (CNN) is used to learn an Euclidean embedding for face images. The key contribution of FaceNet is introduction of the triplet loss [37] by which the CNN network weights are optimized until the features belonging to each identity lie closer compared to features from different identities. Although this work is suitable for face recognition, it can be naturally applied to person ReID task which is very similar to person recognition. The main difficulty of learning person ReID models using the triplet loss is the mining of hard triplets, as otherwise it will frequently produce disappointing results, or even worse, selecting over-hard triplets will result in an unstable training process [7]. The main difficulty of exploiting triplet loss [22, 25, 7] is that the “hard” examples are often not chosen properly with a good criterion to explicitly define what “good” hard triplets are. On the other hand, the triplet loss has its own advantages: it allows us to perform end-to-end learning between the input image and the desired embedding space. Accordingly, we can simply compare people by computing the Euclidean distance of their embeddings.

So far, a large number of variants of the triplet loss have been proposed to improve the ReID performance [19, 9, 5, 20, 4, 33, 25, 28, 3, 15, 7] regardless of the network structure. The triplet loss has become the *de facto* standard of the loss function in ReID deep learning networks. In [36], Deep Anytime Re-ID (DaRe) is proposed

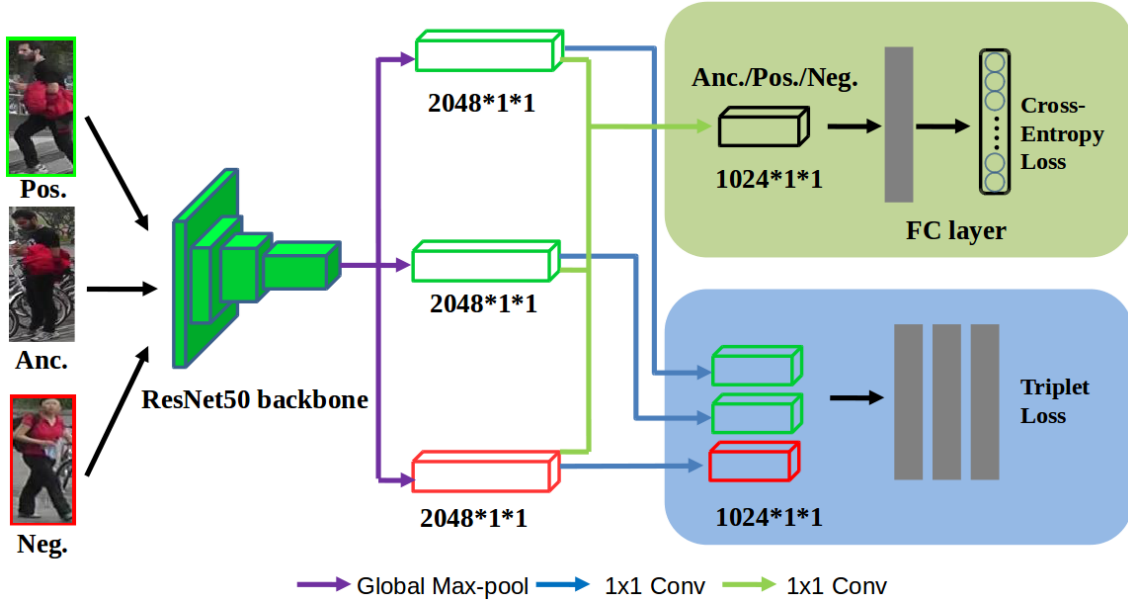


Figure 2. Overview of the proposed ReID network architecture. “Anc.,” “Pos.” and “Neg.” represent anchor image, positive images that belong to the same identity and negative images that belong to different identities, respectively.

which is a resource-aware ReID architecture that combines pooled feature maps from multiple convolutional network layers. The composite loss function consists of per-stage losses and final-stage triplet loss. The ResNet-50 based DaRe approach achieves 88.5% Rank-1 accuracy on the Market-1501 dataset, which is a milestone of the ReID approaches based on global feature. GP-reid [1] discusses a set of good practices for person ReID, especially for using global features and triplet loss, and achieves promising results. In this work, we will show that, by generalizing the triplet loss, it has more potential for learning ReID model by global features.

2.2. Part model

In order to relieve the problem of detection misalignment and background clutter, one strategy is modeling the saliency and applying weights to different local patches for pairwise image matching [42, 24, 45, 35]. Whereas these conventional non deep learning methods heavily rely on handcrafted features, the feature representations are not jointly learned with deep network weights. Thus the solution is not optimal. Recently, a rich body of works have tried to utilize local features in deep learning networks, with the entire CNN parameters being optimized in an end-to-end manner [11, 41, 27, 4, 13, 31, 40, 38, 16, 14].

The main idea of attention model is to evaluate region-level or pixel-level attention map, and implement the importance weighing on feature maps in the middle of the CNN network before global pooling. For region-level attention [11, 41, 27], some works utilize empirical knowledge about

human bodies [4, 13, 31, 39], some acquire region by region proposal methods [38, 11] while others do not rely on the structural information or region proposal but the attention task is achieved during deep learning [27, 40]. In order to further reduce the impact of the background clutter, some attention models are proposed to locate the body part in either middle-level or fine-grained pixel-level [41, 16, 15, 14]. The attention models typically improve ReID performance but require more computation and memory. Additionally, the customized layer of the attention model is not convenient to deploy in different deep learning frameworks, and may need a CUDA expert for implementation.

As an alternative to implement part models, a multi-branch architecture has been proposed to learn an ensemble of network branches which improves the accuracy compared with any single branch setting [39, 31, 34, 14, 2]. A typical work is Part-based Convolutional Baseline (PCB) [31] which applies uniform partition strategy and concatenate region-level local features to form the output composite feature. With the multi-branch architecture, PCB serves as a strong baseline for person ReID. The authors of [14] proposed a multi-branch architecture HA-CNN in which the global branch learns the global feature while each of the three local branches aims to learn the discriminative local features for its corresponding image regions. In view of better utilizing the local features, Deep-Person [2] is proposed to model the spatial dependency of body parts by Long Short-Term Memory (LSTM) in an end-to-end way. The recent work Multiple Granularity Network (MGN) [34] consists of one global and two local branches from *res_conv4*

layer with independent parameters, which can boost each other. MGN can achieve outstanding performance exceeding all previous methods, achieving a milestone of 96.6% Rank-1 accuracy on Market-1501 dataset with a reranking technique. However, the multi-branch architecture usually requires even more computation and memory resources than the part-model based attention methods impeding its practicality in deployment.

3. Learning Composite Feature Embedding

3.1. Network Architecture

In the proposed plain CNN architecture, the ResNet-50 [6] backbone is used for learning the main discriminative ability. The architecture is shown in Fig. 2, where the feature vectors after global pooling are fed to 1×1 convolution, producing 1024-dim features. These features are evaluated using cross-entropy loss and triplet loss, respectively, and concatenated to form the final 2048-dim feature embeddings. The details of loss function and optimization will be discussed in subsection 3.2 and 3.3.

We have conducted preliminary experiments on a single embedding, i.e. the 2048-dim feature after global pooling, with both losses. However, the performance is not as good as training two separate embeddings with the two different loss functions respectively. The main reason is that cross-entropy loss and triplet loss are formulated quite differently, and two heads after global pooling are necessary to boost each other.

3.2. Loss Function for Progressive Learning

As commonly defined in the triplet loss based feature embedding methods [22, 25, 7], the goal of metric embedding learning is to learn a mapping from image data to semantic features. We use θ to denote the network parameters. The function $g(\theta)$ is usually implemented using CNN, which is a non-linear mapping. The metric measure is defined as $D_{i,j} = D(g_\theta(\mathbf{u}), g_\theta(\mathbf{v})) : \mathbb{R}^D \times \mathbb{R}^D \rightarrow R$.

The original form of triplet loss is defined as a large margin nearest neighbor (LMNN) loss [37]:

$$\mathcal{L}_{LMNN}(\theta; X) = (1 - \mu) \sum_{i,j \in C(i)} D_{i,j} \quad (1)$$

$$+ \mu \sum_{\substack{a,b,n \\ y_a=y_b \neq y_n}} [m + D_{a,b} - D_{a,n}]$$

where a and b denotes samples in the same class, and μ and m denote the weighting factor and the margin parameter, respectively. The LMNN loss is essentially a weighted sum of the intra-class Euclidean loss and a variation of the hinge loss.

Hermans et al. [7] extended triplet loss by introducing

the ‘‘batch hard’’ triplet loss which is defined as follows:

$$\mathcal{L}_{BH}(\theta; X) = \sum_{l=1}^P \sum_{\substack{a,b \\ y_a=y_b=l}} \left[m + \max D_{a,b} - \min_{y_n \neq y_a} D_{a,n} \right]_+ \quad (2)$$

where a and b belongs to the same label $y_a \in [1, \dots, P]$, n belongs to a different label with $y_n \neq y_a$. Each label contains K images, forming a batch of $P \times K$ images for training. Note that the batch parameters K and P are constrained by the memory size, which may limit the discriminative ability of the triplet loss strategy. The selected triplets are derived from a small subset of the input data, thus the ‘‘hardest’’ (defined by max and min operations for hardest positive and hardest negative, respectively) can be considered as moderate triplets, which is neither too hard nor too easy for learning with the triplet loss.

In this work, we introduce two **progressive parameters** p and k to control the optimization of triplet loss. Suppose $k \in [1, \dots, K]$, $p \in [1, \dots, P]$, and $\text{Largest}^k(\cdot)$ and $\text{Smallest}^p(\cdot)$ denote the operations to find the k -th largest value of $D_{a,b}$ in the batch and p -th smallest values of $D_{a,n}$, respectively. Then we can generalize the batch hard triplet loss as

$$\mathcal{L}_{GBH}^{k,p}(\theta; X) = \sum_{l=1}^P \sum_{\substack{a,b \\ y_a=y_b=l}} \ln \left(1 + e^{m+T_{k,p}(a,b,n)} \right) \quad (3)$$

$$T_{k,p}(a, b, n) = \text{Largest}^k(D_{a,b}) - \text{Smallest}^p(D_{a,n}) \quad (4)$$

The generalized batch hard loss can define triplets at any hard level, by adjusting the parameters k and p . When $k = p = 1$ the generalized batch hard loss is exactly the same as the batch hard loss defined in Eq. 2. When $k > 1$, easier examples are selected for training, thus the unstable training situation is alleviated.

Our final objective is the composite loss with the cross-entropy loss and the generalized batch hard triplet loss as follows:

$$\mathcal{L}^{k,p}(\theta; X) = \mathcal{L}_{softmax}(\theta; X) + \lambda \mathcal{L}_{GBH}^{k,p}(\theta; X) \quad (5)$$

where λ is a predefined weight for generalized triplet loss as an regularization to the conventional cross-entropy loss. In order to determine its value, we have made a joint Bayesian optimization on parameters in subsection 3.3, and the $\lambda \in [0, 2]$ is set dynamically.

In practice, our loss function can be calculated efficiently. Following [7], we form batches by randomly sampling P classes and randomly select K images of each class. Given PK embeddings, we can compute their pairwise distance and sort them in $O(PK \log(PK))$. Then for each sample, we can select the k -th largest value from all positive distances $D_{a,b}$ with $y_a = y_b$, and p -th smallest value

from all negative distances $D_{a,n}$ with $y_a \neq y_n$. In our experiments PK is as small as 128, for which the sorting algorithm finishes in a short time. Overall our computation cost is comparable with that in [7].

3.3. Progressive Learning Based on Bayesian Optimization

As we can see from the previous section, the progressive parameters p and k are crucial to train the ReID model. When $k = 8$, the optimizer selects easy examples for every batch. When $k = 1$, the hardest example is selected for optimization.

Intuitively we could choose $k = 8$ at the beginning of the optimization and then $k = 1$ later for progressive learning. This incremental nature allows the training to first discover a stable solution for easy triplets and then shift attention to increasingly finetune weights to discriminate hard triplets, while avoiding over-hard triplets if they have no benefits. However, such a holistic approach cannot decide when and how often we shall adjust k , and cannot suggest whether we shall adjust other hyper-parameters λ, m accordingly. In this paper, we employ Bayesian optimization [23] to adjust p, k as well as the other hyper-parameters. Bayesian optimization provides a general framework for minimization of non-convex objective functions, by which the parameters can be jointly optimized by iteratively updating the probabilistic model based on previous exploration.

Suppose $\mathbf{w} = (\lambda, m, k, p)$ denotes all the hyper-parameters for our progressive learning. Define $f(\boldsymbol{\theta}; \mathbf{w}; X)$ as the non-linear function that maps CNN parameters $\boldsymbol{\theta}$, hyper-parameters \mathbf{w} , and input data X to the objective function. As Bayesian optimization is used here to determine the hyper-parameters only, $f(\boldsymbol{\theta}; \mathbf{w}; X)$ is briefed as $f(\mathbf{w})$ in this work. Assume $f(\mathbf{w})$ follows a Gaussian process which is parameterized by a mean function $\mu(\cdot)$ and a covariance kernel $K(\mathbf{w}_1, \mathbf{w}_2) : f \sim \mathcal{GP}(\mu(\cdot), K(\cdot, \cdot))$, then its mean and covariance are $\mu(\mathbf{w}) = \mathbb{E}[f(\mathbf{w})]$ and $K(\mathbf{w}_1, \mathbf{w}_2) = \mathbb{E}[(f(\mathbf{w}_1) - \mu(\mathbf{w}_1))(f(\mathbf{w}_2) - \mu(\mathbf{w}_2))]$, respectively. By Gaussian distribution, $K_{\mathbf{B}}(\mathbf{w}_1, \mathbf{w}_2) = \frac{1}{(2\pi)^{\frac{d}{2}} |\mathbf{B}|^{\frac{1}{2}}} \exp(-\frac{1}{2} \mathbf{w}_1^T \mathbf{B}^{-1} \mathbf{w}_2)$, and \mathbf{B} is the bandwidth matrix calculated from given samples.

Denote $\mathbf{w}_i = (\lambda_i, m_i, k_i, p_i)$ as a set of hyper-parameters. For N sets of such parameters we denote $\mathbb{W} = \{\mathbf{w}_1, \mathbf{w}_2, \dots, \mathbf{w}_N\}$, and the corresponding $f(\mathbb{W}) = \{f(\mathbf{w}_1), f(\mathbf{w}_2), \dots, f(\mathbf{w}_N)\}$. The posterior belief of f at a new candidate $\hat{\mathbf{w}}$ is given by

$$\begin{cases} \tilde{f}(\hat{\mathbf{w}}) \sim \mathcal{GP}(\mu(\hat{\mathbf{w}}) + \Delta\mu, \mathcal{K}(\hat{\mathbf{w}}) - \Delta\mathcal{K}) \\ \Delta\mu = \mathcal{K}(\hat{\mathbf{w}}, \mathbb{W}) \mathcal{K}(\mathbb{W})^{-1} (f(\mathbb{W}) - \mu(\mathbb{W})) \\ \Delta\mathcal{K} = \mathcal{K}(\hat{\mathbf{w}}, \mathbb{W}) \mathcal{K}(\mathbb{W})^{-1} \mathcal{K}(\mathbb{W}, \hat{\mathbf{w}}) \end{cases} \quad (6)$$

where $\mathcal{K}(\mathbb{W}) = \mathcal{K}(\mathbb{W}, \mathbb{W})$ for brief.

Algorithm 1 Training the ReID model based on PLA.

Input: A fixed-size mini-batch consisting of $P = 16$ randomly selected identities and $K = 8$ randomly selected images per identity from the training set.

Output: The optimal hyperparameter \mathbf{w}^* along with the well trained CNN.

Initialization: Randomly initialize N sets of hyper-parameters $\mathbb{W} = \{\mathbf{w}_1, \mathbf{w}_2, \dots, \mathbf{w}_N\}$ where $\mathbf{w}_i = (\lambda_i, m_i, k_i, p_i)$, $\lambda_i \in [0, 2]$, $m_i \in [-0.1, 0.3]$, $k_i \in [1, 8]$, $p_i \in [1, 16]$ for $i = 1, \dots, N$.

Repeat

for each hyperparameter $i = 1$ to N **do**

Exploration: Backpropagate CNN in 20 epochs and evaluate the loss \mathcal{L} according to Eq. 3 and Eq. 5, and evaluate the Bayesian objective $f(\mathbf{w}_i)$.

Restoration: CNN weights are restored to that before 20 epochs of exploration.

end for

Exploitation: Based on $f(\mathbb{W})$, obtain a new improved candidate \mathbf{w}' and update Gaussian process according to Eq. 6 and Eq. 8, and add \mathbf{w}' to \mathbb{W} .

Backpropagate to update CNN weights for 300 epochs based on the new hyperparameter $\hat{\mathbf{w}}$ and the feed-forward loss \mathcal{L} ;

Save the model with lowest loss \mathcal{L} for the current hyperparameter $\hat{\mathbf{w}}$;

Until maximum epochs ($M = 3,000$) reached

Let \mathbf{w}' denote the best candidate evaluated so far, then the expected improvement of a candidate $\hat{\mathbf{w}}$ is defined as

$$\mathcal{EI}(\hat{\mathbf{w}}) = \mathbb{E} \left[f(\mathbf{w}') - \tilde{f}(\hat{\mathbf{w}}) \right]_+ \quad (7)$$

which can be efficiently computed in closed form:

$$\mathcal{EI}(\hat{\mathbf{w}}) = (\mathcal{K}(\hat{\mathbf{w}}) - \Delta\mathcal{K})^{\frac{1}{2}} (Z\Phi(Z) + \phi(Z)) \quad (8)$$

where $Z = (\tilde{\mu}_f(\hat{\mathbf{w}}) - f(\mathbf{w}')) / (\mathcal{K}(\hat{\mathbf{w}}) - \Delta\mathcal{K})^{\frac{1}{2}}$, and $\Phi(\cdot)$ and $\phi(\cdot)$ are the standard normal cumulative distribution function and probability density function, respectively.

In each iteration of Bayesian optimization, a fixed-size of new hyper-parameters are sampled where the one that maximizes $\mathcal{EI}(\hat{\mathbf{w}})$ is chosen, and \mathbb{W} is updated accordingly. For more details, one can refer to [26].

Then the objective of the Bayesian optimization is determined by loss function in the last section. In practice, we find when the composite loss decreases in a speed of relatively 15% of the previous loss, the training is healthy with good hyper-parameters. So in our system, Bayesian optimization minimizes the following objective function:

$$f(\mathbf{w}) = \left| \frac{\bar{\mathcal{L}}_t^{k,p}(\boldsymbol{\theta}; \mathbf{w}; X) - \bar{\mathcal{L}}_{t'}^{k,p}(\boldsymbol{\theta}; \mathbf{w}; X)}{\bar{\mathcal{L}}_t^{k,p}(\boldsymbol{\theta}; \mathbf{w}; X)} - \mathcal{ED} \right| \quad (9)$$

where $\bar{\mathcal{L}}_t^{k,p}(\theta; \mathbf{w}; X)$ and $\bar{\mathcal{L}}_{t'}^{k,p}(\theta; \mathbf{w}; X)$ are the average CNN loss functions in the first 10 epochs and second 10 epochs of the t -th exploration in Algorithm 1, $\mathcal{E}\mathcal{D}$ is the expected drop rate of the loss, which is empirically set to 0.15 as a healthy training process.

The overall PLA is shown in Algorithm 1. The whole training procedure is end-to-end with the backbone of ResNet-50 is pretrained from ImageNet, and the 1×1 convolutions after global pooling are randomly initialized. Based on the trained PLA model, a 2048-dim feature will be generated from a query image to match features extracted from the gallery images.

4. Experiments

In this section, we first introduce datasets and evaluation protocols used in our experiments, then parameter setting and performance analysis are provided. This is followed by experimental results compared with other state-of-the-art methods. A reranking technique [47] is a popular option to post-processing to improve the ReID precision.

4.1. Datasets and Protocols

We perform all the experiments on three commonly used benchmarks: Market-1501 [43], DukeMTMC-ReID [21] (briefed as DukeMTMC), and CUHK03(D) & CUHK03(L) [12] datasets. These ReID datasets are summarized in Table 1.

Dataset	Market1501	DukeMTMC	CUHK03(D/L)
Identities	1,501	1,812	1,360
Bboxes	32,668	36,411	13,164
Camera	6	8	6
Train images	12,936	16,522	7,365/7,368
Train ids	751	702	767
Query images	3,368	2,228	1,400
Query ids	750	702	700
Gallery images	19,732	17,661	5,332

Table 1. ReID Benchmark datasets used in our experiments.

We report Cumulative Matching Characteristics (CMC) at Rank-1 accuracy and mean average precision (mAP) for all the three datasets. On Market-1501 dataset, we evaluate our method on two evaluation protocols: single-query using one image as query, and multiple-query using more than one images of one person in dataset to query. On CUHK03 dataset, we follow the setting in [47] that splits dataset into 767 training IDs and 700 test IDs, and report the performance on the test set with unknown IDs. Note that this protocol is different from the old setting [17, 29] with 1160 training IDs and 100 test IDs, which the average of 20 trials of the random samples. Although the old setting often leads to higher mAP or Rank-1 scores, it is not objective and suffers from the randomness. In this paper, we only compare

with the results using the new setting as meaningful baselines.

4.2. Implementation Details

Similar to [7], all images are resized to 256×128 resolution as a tradeoff between ReID efficiency and accuracy. For online image augmentation, we first amplify by a factor 1.125, then do a 256×128 random crop and a random horizontal flip in the training process. Random erasing [48] is also used which randomly ($p = 0.5$) masks parts of person to simulate the cases of occlusion and missing body parts in a dataset. We apply 10-crop test time augmentation for evaluations. We use Principle Component Analysis (PCA) to reduce the 2048-dim feature embedding to 512-dim as post processing. As to mini-batch size, according to preliminary experiments, increasing the number of images per person can benefit the final accuracy of the trained model. Moreover, by using the proposed progressive learning algorithm, images from the same person are required to contain various levels of hard examples to optimize the training process. Considering the GPU memory, we set $P = 16$, $K = 8$ to generate image batches to feed into the model training process which is different from [7] with $P = 18$ and $K = 4$. We use Adam [10] as the optimizer and set $\beta_1 = 0.9$ within 150 epochs and $\beta_1 = 0.5$ for remaining epochs, and $\beta_2 = 0.999$. We adjust the learning rate training schedule as proposed by [7]:

$$\alpha(e) = \begin{cases} \alpha_0 & \text{if } e \leq e_0 \\ \alpha_0 \times 0.001^{\frac{e-e_0}{e_1-e_0}} & \text{if } e_0 \leq e \leq e_1 \end{cases} \quad (10)$$

where we set $\alpha_0 = 3 \times 10^{-4}$, $e_0 = 150$ epochs, and $e_1 = 300$ epochs.

The simulation environments are given as follows: Ubuntu 16.04, Intel® Xeon® CPU E5-2667 v4 @ 3.20GHz \times 32, 64GB RAM, and NVIDIA® GeForce® GTX 1080 Ti/PCIe/SSE2.

4.3. Ablation Study

In the proposed network structure, after global max pooling of the ResNet-50 backbone, the network is split into two heads, one for triplet loss and the other for cross-entropy loss. Considering that triplet loss is a ranking function, while cross-entropy loss is a classification target, their feature representations are different. Combining them should have richer feature representation than each of them alone. In our testing process, we used three variants of the network head: 2048-dim feature with cross-entropy loss only, 2048-dim feature with triplet loss only, and the 2048-dim feature (concatenation of two 1024-dim feature embeddings).

Figure 3 shows the effectiveness of loss concatenation and progressive learning on Market-1501 dataset in terms of mAP and Rank-1 accuracy. The 2048-dim feature with

Category	Methods	Market1501(SQ)		Market1501(MQ)		CUHK03(D)		CUHK03(L)		DukeMTMC	
		mAP	Rank-1	mAP	Rank-1	mAP	Rank-1	mAP	Rank-1	mAP	Rank-1
part	HA-CNN[14]	75.7	91.2	82.8	93.8	38.6	41.7	41.0	44.4	63.8	80.5
	Deep-Person[2]	79.6	92.3	85.1	94.5	-	-	-	-	64.8	80.9
	PCB[31]	77.4	92.3	-	-	54.2	61.3	-	-	66.1	81.7
	PCB+RPP[31]	81.6	93.8	-	-	57.5	63.7	-	-	69.2	83.3
	Aligned-ReID[39]	82.3	92.6	-	-	-	-	-	-	-	-
	MGN[34]	86.9	95.7	90.7	96.9	66.0	66.8	67.4	68.0	78.4	88.7
global	SVDNet[30]	62.1	82.3	-	-	37.2	41.5	37.8	40.9	56.8	76.7
	TriNet[7]	69.1	84.9	76.4	90.5	-	-	-	-	-	-
	GP-reid[1]	81.2	92.2	82.8	93.8	-	-	-	-	72.8	85.2
	DaRe[36]	74.2	88.5	-	-	58.1	61.6	60.2	64.5	63.0	79.1
	PLA	83.6	93.7	88.4	95.2	63.2	67.2	67.5	71.5	72.5	84.3
RK	Trinet [7]	81.1	86.7	87.2	91.8	-	-	-	-	-	-
	DaRe [36]	85.9	90.8	-	-	71.2	69.8	73.7	72.9	79.6	84.4
	MGN [34]	94.2	96.6	95.9	97.1	-	-	-	-	-	-
	PLA	89.4	94.7	92.9	95.7	77.2	75.5	81.0	79.6	80.1	87.0

Table 2. Comparing PLA with different global and part models on all datasets. ‘‘RK’’ stands for reranking.

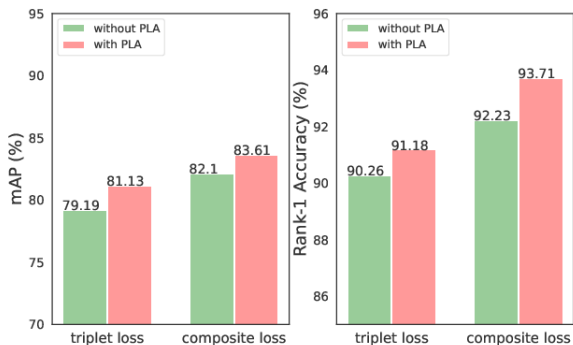


Figure 3. Using PLA on Market-1501 dataset. It can be seen PLA consistently improves the performance of both triplet loss and composite loss under every evaluation metrics.

cross-entropy loss alone achieved 70.4% and 85.5% in terms of mAP and Rank-1 accuracy, respectively. With the proposed PLA, the triplet feature embedding achieved mAP and Rank-1 accuracy of 81.1% and 91.2%, respectively, outperforming the accuracies using each type of loss with 2048-dim feature without PLA. Coupling the feature concatenation method, the proposed progressive learning algorithm brought significant improvements 4.4% for mAP and 3.5% for Rank-1 compared to using triplet loss alone on Market-1501 dataset. We found progressive learning and concatenated feature embedding, when used together, produced the best results. This indicates the progressive learning is effective to learn more accurate and robust representation of person identities.

4.4. Compare with the State-of-the-arts

We compare the proposed ReID approach with various ReID approaches based on both global models and part models. The global model based approaches include: SVDNet [30], TriNet [7], GP-reid [1], and ResNet-50 based DaRe [36]. The part model based approaches include: HA-CNN [14], PCB [31], Aligned-ReID [39], Deep-Person [2] and MGN [34].

The comparison results over state-of-the-art method with global models are shown in Table 2. Without the reranking technique, GP-reid [1] achieved a good performance as it properly makes use of many existing techniques. The proposed PLA consistently outperforms all other global feature models by a large margin without reranking technique, except for GP-reid. PLA outperforms GP-reid in terms of mAP accuracy by 2.4% and 5.6% on Market-1501 dataset with single query mode and multiple query mode, respectively. However, GP-reid slightly outperforms PLA in terms of mAP and Rank-1 accuracy by 0.3% and 0.9%, respectively, on DukeMTMC dataset. Note that in this work the learning rate schedule is uniform in all experiments and not specially tailored for DukeMTMC dataset. We can observe that the proposed PLA consistently outperforms all other methods with reranking by a large margin. PLA outperforms DaRe in terms of mAP by 9.4%, 5.1%, 7.3% and 9.5% without reranking on Market-1501(SQ), CUHK03(D), CUHK03(L) and DukeMTMC datasets respectively. Overall, the proposed PLA has the best performance over other global models.

Although the proposed approach is within the scope of global feature model, we also compare it with the accuracies produced by multi-branch part models, as shown in Table 2 for all datasets. In Table 2, it is obvious that MGN

achieves the highest accuracies among all part models on Market-1501 dataset without reranking technique. It is evident that the proposed PLA outperforms all previous works except for MGN. In terms of Rank-1 accuracy performance without reranking, PLA is overall comparable with MGN in terms of Rank-1 accuracy: MGN exceeds PLA by 2% and 4.3% on Market-1501(SQ) and DukeMTMC dataset respectively, while MGN is inferior than PLA by 0.4% and 3.5% on CUHK03(D) and CUHK03(L) datasets. We can also observe that with reranking, PLA outperforms DaRe by a large margin achieving the highest mAP and Rank-1 values ever publicly reported on the CUHK03(D) and CUHK03(L) datasets.

4.5. Computational Cost and Inference Memory

The proposed PLA is designed for resource-aware ReID, and a good trade off between accuracy and efficiency is expected. The computational cost is reported with respect to the total number of basic operations, i.e. multiplications and additions (Mul-Add), which is proportional to the actual running timing. Reranking is not included in the Mul-Add calculation. HA-CNN [14], ResNet-50 based DaRe [36], PCB(RPP) [31] and MGN [34] are chosen to be compared with the proposed PLA for their good performance.

The graph of accuracy vs. efficiency is shown in Fig. 4. Accuracy reported is the average mAP on Market-1501, CUHK03(D), CUHK03(L) and DukeMTMC datasets without reranking. We observe that the proposed PLA achieves significantly higher accuracies than HA-CNN and DaRe. In particular, PLA achieves slightly higher accuracy than PCB which is a strong part model baseline for ReID, yet saving more than 30% computation cost. MGN outperforms PLA and PCB in accuracy by a small margin, however, it has a tremendous Mul-Add of roughly 2.3×10^{10} which is about 3 times of PLA.

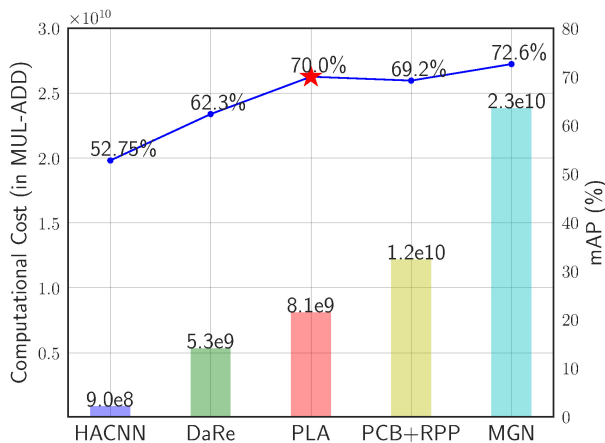


Figure 4. Accuracy vs. computation cost (number of Mul-Add). Accuracy is reported as the average mAP on all datasets.

The graph of accuracy vs. inference memory is shown in Fig. 5. It is evident that the trade off situation is similar to that in Fig. 4. Although HA-CNN is a multi-branch part model, the input size is fairly small compared with other approaches, making it the most lightweight approach. HA-CNN shows good accuracy on Market-1501 dataset but exhibits rather low accuracies on CUHK and DukeMTMC datasets, as shown in Table 2. MGN outperforms all others in terms of accuracy, but it is more than 2 times of the PLA inference memory. Accordingly, it requires at least 11.6GB memory for inference with a commonly used batch size of 64, which even cannot be loaded using GTX 1080Ti (11.17GB). Note that even though network acceleration techniques *e.g.* TensorRT [18] and network compression techniques *e.g.* [32] can be used to save Mul-Add and reduce inference memory, respectively, for strong part models including PCB and MGN, they will also benefit PLA by similar acceleration and compression ratios since ResNet-50 is the backbone of all these networks.

It is evident that in both charts in Fig. 4 and Fig. 5, our method is outstanding in its accuracy and resource balance: the models with less resource requirements exhibit obvious lower or unstable accuracy while those with slightly higher accuracy will consume unnecessarily much more computational cost and inference memory.

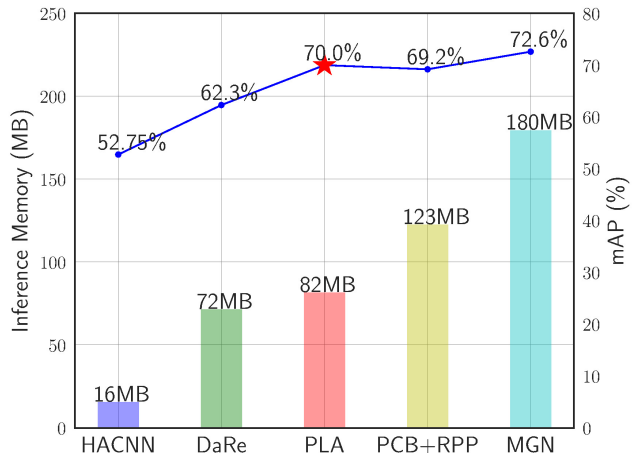


Figure 5. Accuracy vs. inference memory (MB). Accuracy is reported as the average mAP on all datasets.

5. Conclusions

Different from the recent trend of employing part models to improve the accuracy at the cost of more computation and memory, this paper developed a novel optimization algorithm to find efficient models in a single main branch network with competitive performance. The core idea is to design a progressive triplet loss to explore the power of

deep CNN representation, which is efficient for model inference. Compared to the most state-of-the-art algorithms, e.g. MGN, which produces slightly higher accuracy than PLA on average, PLA saves 65% computational cost and 54% inference memory. Experimental results show that the proposed PLA achieves the excellent tradeoff between accuracy and efficiency, and we hope this work could motivate more research work to find efficient models with high performance and lower consumption.

References

- [1] J. Almazan, B. Gajic, N. Murray, and D. Larlus. Re-id done right: towards good practices for person re-identification. *arXiv preprint arXiv:1801.05339*, 2018.
- [2] X. Bai, M. Yang, T. Huang, Z. Dou, R. Yu, and Y. Xu. Deep-person: Learning discriminative deep features for person re-identification. *arXiv preprint arXiv:1711.10658*, 2017.
- [3] W. Chen, X. Chen, J. Zhang, and K. Huang. A multi-task deep network for person re-identification. In *AAAI*, pages 3988–3994, 2017.
- [4] D. Cheng, Y. Gong, S. Zhou, J. Wang, and N. Zheng. Person re-identification by multi-channel parts-based cnn with improved triplet loss function. In *Computer Vision and Pattern Recognition*, pages 1335–1344, 2016.
- [5] S. Ding, L. Lin, G. Wang, and H. Chao. Deep feature learning with relative distance comparison for person re-identification. *Pattern Recognition*, 48(10):2993–3003, 2015.
- [6] K. He, X. Zhang, S. Ren, and J. Sun. Deep residual learning for image recognition. In *Proceedings of the IEEE conference on computer vision and pattern recognition*, pages 770–778, 2016.
- [7] A. Hermans, L. Beyer, and B. Leibe. In defense of the triplet loss for person re-identification. *arXiv preprint arXiv:1703.07737*, 2017.
- [8] C. C.-H. Hsu, M. Y.-C. Wang, H. C. Shen, R. H.-C. Chiang, and C. H. Wen. Fallcare+: An iot surveillance system for fall detection. In *2017 International Conference on Applied System Innovation (ICASI)*, pages 921–922. IEEE, 2017.
- [9] S. Khamsi, C.-H. Kuo, V. K. Singh, V. D. Shet, and L. S. Davis. Joint learning for attribute-consistent person re-identification. In *European Conference on Computer Vision*, pages 134–146. Springer, 2014.
- [10] D. P. Kingma and J. Ba. Adam: A method for stochastic optimization. *arXiv preprint arXiv:1412.6980*, 2014.
- [11] D. Li, X. Chen, Z. Zhang, and K. Huang. Learning deep context-aware features over body and latent parts for person re-identification. In *Proceedings of the IEEE Conference on Computer Vision and Pattern Recognition*, pages 384–393, 2017.
- [12] W. Li, R. Zhao, T. Xiao, and X. Wang. Deep-reid: Deep filter pairing neural network for person re-identification. In *Proceedings of the IEEE Conference on Computer Vision and Pattern Recognition*, pages 152–159, 2014.
- [13] W. Li, X. Zhu, and S. Gong. Person re-identification by deep joint learning of multi-loss classification. *arXiv preprint arXiv:1705.04724*, 2017.
- [14] W. Li, X. Zhu, and S. Gong. Harmonious attention network for person re-identification. In *Computer Vision and Pattern Recognition*, volume 1, page 2, 2018.
- [15] H. Liu, J. Feng, M. Qi, J. Jiang, and S. Yan. End-to-end comparative attention networks for person re-identification. *IEEE Transactions on Image Processing*, PP(99):1–1, 2016.
- [16] X. Liu, H. Zhao, M. Tian, L. Sheng, J. Shao, J. Yan, and X. Wang. Hydraplus-net: Attentive deep features for pedestrian analysis. In *Proceedings of the IEEE international conference on computer vision*, pages 1–9, 2017.
- [17] C. Mao, Y. Li, Z. Zhang, Y. Zhang, and X. Li. Pyramid person matching network for person re-identification. 2018.
- [18] NVIDIA. NVIDIA TensorRT: Programmable Inference Accelerator. <https://developer.nvidia.com/tensorrt>, 2018.
- [19] H. Oh Song, Y. Xiang, S. Jegelka, and S. Savarese. Deep metric learning via lifted structured feature embedding. In *Proceedings of the IEEE Conference on Computer Vision and Pattern Recognition*, pages 4004–4012, 2016.
- [20] S. Paisitkriangkrai, C. Shen, and A. Van Den Hengel. Learning to rank in person re-identification with metric ensembles. In *Proceedings of the IEEE Conference on Computer Vision and Pattern Recognition*, pages 1846–1855, 2015.
- [21] E. Ristani, F. Solera, R. Zou, R. Cucchiara, and C. Tomasi. Performance measures and a data set for multi-target, multi-camera tracking. In *European Conference on Computer Vision workshop on Benchmarking Multi-Target Tracking*, 2016.
- [22] F. Schroff, D. Kalenichenko, and J. Philbin. Facenet: A unified embedding for face recognition and clustering. In *Proceedings of the IEEE conference on computer vision and pattern recognition*, pages 815–823, 2015.

- [23] B. Shahriari, K. Swersky, Z. Wang, R. P. Adams, and N. De Freitas. Taking the human out of the loop: A review of bayesian optimization. *Proceedings of the IEEE*, 104(1):148–175, 2016.
- [24] Y. Shen, W. Lin, J. Yan, M. Xu, J. Wu, and J. Wang. Person re-identification with correspondence structure learning. In *Proceedings of the IEEE International Conference on Computer Vision*, pages 3200–3208, 2015.
- [25] H. Shi, Y. Yang, X. Zhu, S. Liao, Z. Lei, W. Zheng, and S. Z. Li. Embedding deep metric for person re-identification: A study against large variations. In *European Conference on Computer Vision*, pages 732–748. Springer, 2016.
- [26] J. Snoek, H. Larochelle, and R. P. Adams. Practical bayesian optimization of machine learning algorithms. In *Advances in neural information processing systems*, pages 2951–2959, 2012.
- [27] C. Su, J. Li, S. Zhang, J. Xing, W. Gao, and Q. Tian. Pose-driven deep convolutional model for person re-identification. In *IEEE International Conference on Computer Vision*, pages 3980–3989. IEEE, 2017.
- [28] C. Su, S. Zhang, J. Xing, W. Gao, and Q. Tian. Deep attributes driven multi-camera person re-identification. In *European Conference on Computer Vision*, pages 475–491, 2016.
- [29] Y. Suh, J. Wang, S. Tang, T. Mei, and K. M. Lee. Part-aligned bilinear representations for person re-identification. 2018.
- [30] Y. Sun, L. Zheng, W. Deng, and S. Wang. Svdnet for pedestrian retrieval. In *IEEE International Conference on Computer Vision*, pages 3820–3828, 2017.
- [31] Y. Sun, L. Zheng, Y. Yang, Q. Tian, and S. Wang. Beyond part models: Person retrieval with refined part pooling. *arXiv preprint arXiv:1711.09349*, 2017.
- [32] D. Wang, L. Zhou, X. Zhang, X. Bai, and J. Zhou. Exploring linear relationship in feature map subspace for convnets compression. *arXiv preprint arXiv:1803.05729*, 2018.
- [33] F. Wang, W. Zuo, L. Lin, D. Zhang, and L. Zhang. Joint learning of single-image and cross-image representations for person re-identification. In *Computer Vision and Pattern Recognition*, pages 1288–1296, 2016.
- [34] G. Wang, Y. Yuan, X. Chen, J. Li, and X. Zhou. Learning discriminative features with multiple granularities for person re-identification. In *Proceedings of the 26th ACM international conference on Multimedia*, pages 274–282, 2018.
- [35] H. Wang, S. Gong, and T. Xiang. Unsupervised learning of generative topic saliency for person re-identification. *Queens Mary Computer Vision Group, University of London*, 2014.
- [36] Y. Wang, L. Wang, Y. You, X. Zou, V. Chen, S. Li, G. Huang, B. Hariharan, and K. Q. Weinberger. Resource aware person re-identification across multiple resolutions. In *Proceedings of the IEEE Conference on Computer Vision and Pattern Recognition*, pages 8042–8051, 2018.
- [37] K. Q. Weinberger, J. Blitzer, and L. K. Saul. Distance metric learning for large margin nearest neighbor classification. In *Advances in neural information processing systems*, pages 1473–1480, 2006.
- [38] H. Yao, S. Zhang, Y. Zhang, J. Li, and Q. Tian. Deep representation learning with part loss for person re-identification. *arXiv preprint arXiv:1707.00798*, 2017.
- [39] X. Zhang, H. Luo, X. Fan, W. Xiang, Y. Sun, Q. Xiao, W. Jiang, C. Zhang, and J. Sun. Aligned-dreid: Surpassing human-level performance in person re-identification. *arXiv preprint arXiv:1711.08184*, 2017.
- [40] H. Zhao, M. Tian, S. Sun, J. Shao, J. Yan, S. Yi, X. Wang, and X. Tang. Spindle net: Person re-identification with human body region guided feature decomposition and fusion. In *Computer Vision and Pattern Recognition*, pages 907–915, 2017.
- [41] L. Zhao, X. Li, Y. Zhuang, and J. Wang. Deeply-learned part-aligned representations for person re-identification. In *IEEE International Conference on Computer Vision*, pages 3239–3248, 2017.
- [42] R. Zhao, W. Ouyang, and X. Wang. Unsupervised saliency learning for person re-identification. In *Proceedings of the IEEE Conference on Computer Vision and Pattern Recognition*, pages 3586–3593, 2013.
- [43] L. Zheng, L. Shen, L. Tian, S. Wang, J. Wang, and Q. Tian. Scalable person re-identification: A benchmark. In *Proceedings of the IEEE International Conference on Computer Vision*, pages 1116–1124, 2015.
- [44] L. Zheng, Y. Yang, and A. G. Hauptmann. Person re-identification: Past, present and future. *arXiv preprint arXiv:1610.02984*, 2016.
- [45] W. S. Zheng, X. Li, T. Xiang, S. Liao, J. Lai, and S. Gong. Partial person re-identification. In *IEEE International Conference on Computer Vision*, pages 4678–4686, 2016.
- [46] Z. Zheng, L. Zheng, and Y. Yang. A discriminatively learned cnn embedding for person re-identification. *Acm Transactions on Multimedia Computing Communications & Applications*, 14(1), 2016.

- [47] Z. Zhong, L. Zheng, D. Cao, and S. Li. Re-ranking person re-identification with k-reciprocal encoding. In *IEEE Conference on Computer Vision and Pattern Recognition*, pages 3652–3661, 2017.
- [48] Z. Zhong, L. Zheng, G. Kang, S. Li, and Y. Yang. Random erasing data augmentation. *arXiv preprint arXiv:1708.04896*, 2017.